Syntheses and X-ray Crystal Structures of Di- and Trinuclear Trithiolate−Thioether-Bridged Complexes of Ruthenium. Electrochemistry of Mixed-Valence Triruthenium Complexes

Richard Y. C. Shin, Sin Yee Ng, Geok Kheng Tan, Lip Lin Koh, Soo Beng Khoo, and Lai Yoong Goh*

Department of Chemistry, National University of Singapore, Kent Ridge, Singapore 119260

Richard D. Webster

Research School of Chemistry, Australian National University, Canberra, Australian Capital Territory 0200, Australia

Received September 25, 2003

The reaction of [(HMB)Ru^{II}(κ^3SSS'-tpdt)] (**1**; HMB = η^6-C_6Me_6; tpdt = $S(CH_2CH_2S^-)_2$) with 0.5 molar equiv of [Cp*$Ru^{III}Cl_2]_2$ (**2A**; Cp* = η^5-C_5Me_5) at ambient temperature gives a mixture of products consisting of the dinuclear complex [{Ru^{III}(μ-1κ^3SSS':2κ^2SS-tpdt)Cl_2(CH_3-CN)}Cp*Ru^{III}Cl] (**6**; 7%) and trinuclear complexes [{(HMB)Ru^{II}(μ_3-1κ^3SSS':2κS:3κS-tpdt)}-{Cp*Ru^{II}(μ-Cl)}$_2$] (**7**; 13%) and [{(HMB)Ru^{II}(μ-1κ^3SSS':2κ^2SS-tpdt)}Ru^{III}Cl(μ-2κ^3SSS':3κ^2SS-tpdt){Cp*Ru^{III}Cl}]Cl (**8**; 54%). **1** reacts with 1 molar (monomer) equiv of $[Ru^{II}(COD)Cl_2]_n$ at 80 °C to give yellow solids of [(HMB)Ru^{II}(μ-1κ^3SSS':2κ^2SS-tpdt)Ru^{II}(COD)Cl_2] (**10**) in 60% yield. [Cp*Ru^{III}(κ^3SSS'-tpdt)] (**2**) reacts with $[Ru^{II}(COD)Cl_2]_n$ in refluxing acetonitrile or with $(PPh_3)_3Ru^{II}Cl_2$ in MeOH at room temperature to give the dark green trinuclear complex [{Cp*Ru^{III}(μ-1κ^3SSS':2κ^2SS-tpdt)}$_2Ru^{II}$Cl]Cl (**12**) in high yield. Treatment of **8**, **10**, and **12** with NH_4PF_6 in acetonitrile results in facile replacement of one or two chloro ligands with solvent molecules, giving PF_6^- salts of the chloro-bridged species [{(HMB)Ru^{II}(μ-1κ^3SSS':2κ^2SS-tpdt)}Ru^{III}(μ-2κ^3SSS':3κ^2SS-tpdt){Cp*Ru^{III}(μ-Cl)}]$(PF_6)_2$ (**9**), the bis(acetonitrile) derivative [(HMB)Ru^{II}(μ-1κ^3SSS':2κ^2SS-tpdt)Ru^{II}(COD)$(CH_3CN)_2](PF_6)_2$ (**11**), and the mono-(acetonitrile) derivative [{Cp*Ru^{III}(μ-1κ^3SSS':2κ^2SS-tpdt)}$_2Ru^{II}$(CH_3CN)]$(PF_6)_2$ (**13**), respectively. The triruthenium complexes can be electrochemically reduced and oxidized in one and sometimes two successive one-electron steps, with many of the reduced and oxidized species being stable on the cyclic voltammetric time scale at low temperatures (−40 °C) in CH_2Cl_2. The location of the redox-active sites and the extent of delocalization in the species with unpaired electrons are discussed. The X-ray crystal structures of **6** and **7** and the PF_6^- salts of **9, 11**, and **13** are reported. The molecular structure of **7** exhibits a new μ_3-1κ^3SSS':2κS:3κS-bonding mode for the tpdt ligand.

Introduction

Transition-metal complexes containing sulfide and thiolate ligands are of continuing interest because of their biological[1a−d] and industrial significance.[1a,b,e−j] The coordination chemistry of thiolates and dithiolates of alkanes and arenes has been extensively studied. Indeed, there are ample examples of various types of bonding modes of these ligands in metal complexes.[2] However, complexes of tridentate dithiolate−thioether ligands such as 3-thiapentane-1,5-dithiolate, $S(CH_2CH_2S^-)_2$ (tpdt), are rare, especially those in which tpdt adopts a bridging mode, e.g. the μ-1κ^3SSS':2κS-bridging mode illustrated in Chart 1 for complexes such as $Mo(tpdt)_2$,[3a] $Ni_2(tpdt)_2$ and $Pd_3(tpdt)_3$,[3b,c] and $(C_2B_9H_{11})_2In_2$(tpdt).[3d] We recently reported the first tpdt complexes

* To whom correspondence should be addressed. E-mail: chmgohly@nus.edu.sg. Fax: (+65) 6779 1691.

(1) See for instance the following and the references therein: (a) *Transition Metal Sulfur Chemistry-Biological and Industrial Significance*; ACS Symposium Series 653; Stiefel, E. I., Matsumoto, K., Eds.; American Chemical Society: Washington, DC, 1996. (b) Howard, J. B.; Rees, D. C. *Chem. Rev.* **1996**, *96*, 2965. (c) Sellman, D.; Sutter, J. *Acc. Chem. Res.* **1997**, *30*, 460 and references therein. (d) Burgess, B. K.; Lowe, D. J. *Chem. Rev.* **1996**, *96*, 2983. (e) Dubois, M. R. *Chem. Rev.* **1989**, *89*, 1. (f) Curtis, M. D.; Druker, S. H. *J. Am. Chem. Soc.* **1997**, *119*, 1027. (g) Bianchini, C.; Meli, A. *Acc. Chem. Res.* **1998**, *31*, 109. (h) Sánchez-Delgado, R. A. *J. Mol. Catal.* **1994**, *86*, 287.

(2) (a) Müller, A.; Diemann, E. In *Comprehensive Coordination Chemistry*; Wilkinson, G., Gillard, R. D., McCleverty, J. A., Eds.; Pergamon Press: Oxford, U.K., 1987; Vol. 2, Chapter 16.1, pp 526−531, and references therein. (b) Bennett, M. A.; Khan, K.; Wenger, E. In *Comprehensive Organometallic Chemistry II*; Abel, E. W., Stone, F. G. A., Wilkinson, G., Shriver, D. F., Bruce, M. I., Eds.; Pergamon: Oxford, U.K., 1995; Vol. 7, pp 522−523 and references therein. (c) Blower, P. J.; Dilworth, J. R. *Coord. Chem. Rev.* **1987**, *76*, 121. (d) Dance, I. G. *Polyhedron* **1986**, *5*, 1037. (e) Krebs, B.; Henkel, G. *Angew. Chem., Int. Ed. Engl.* **1991**, *30*, 769.

(3) (a) Hyde, J.; Magin, L.; Zubieta, J. A. *J. Chem. Soc., Chem. Commun.* **1980**, 204. (b) Barclay, G. A.; McPartlin, E. M.; Stephenson, N. C. *Inorg. Nucl. Chem. Lett.* **1967**, *3*, 397. (c) Barclay, G. A.; McPartlin, E. M.; Stephenson, N. C. *Aust. J. Chem.* **1968**, *21*, 2669. (d) Kim, J.-H.; Huang, J.-W.; Park, Y.-W.; Do, Y. *Inorg. Chem.* **1999**, *38*, 353.

10.1021/om034189+ CCC: $27.50 © 2004 American Chemical Society
Publication on Web 12/31/2003

Chart 1. μ-1κ^3SSS':2κS-Bonding Mode of tpdt in Di- and Trinuclear Complexes

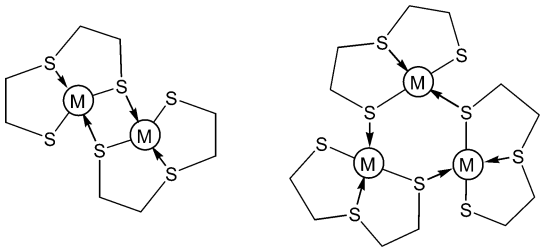

of ruthenium: viz., **1** and **2** containing tpdt in a κ^3SSS'-bonding mode and **3**−**5** containing a hitherto unknown μ-1κ^3SSS':2κ^2SS-bonding mode (eqs i−iii).[4,5] In addition

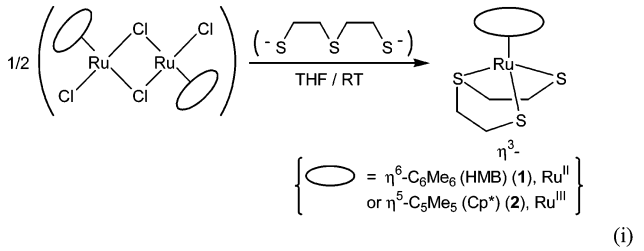

(i)

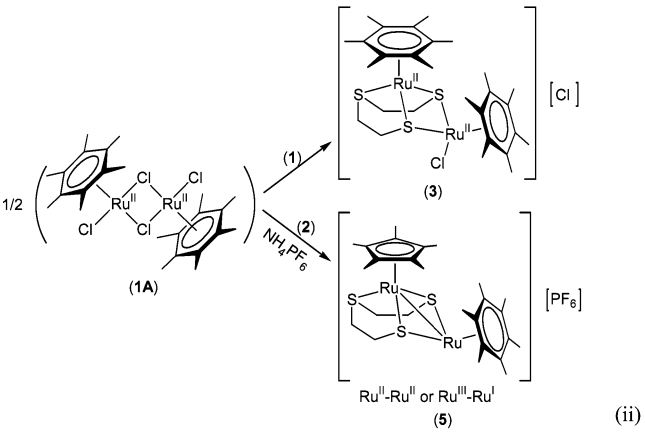

(ii)

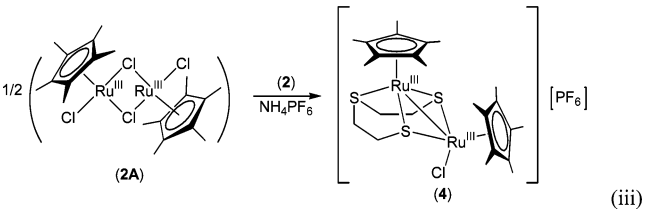

(iii)

to double thiolate bridges as found between the Ru(II)/Ru(II) centers in **3**, **4** also contains a metal−metal bond between the Ru(III)/Ru(III) centers. The "mixed-ring" thiolate-bridged dinuclear complex **5**, obtained from the reaction of **2** with **1A**, is structurally similar to **4**, except that the metal−metal bond here connects either Ru(II)/Ru(II) or Ru(III)/Ru(I) centers (eq ii).[5] It appears that the reaction of **2** with either **1A** or **2A** results in metal−metal-bonded dithiolate-bridged dinuclear derivatives. Examples of metal−metal bonding in thiolate-bridged diruthenium species of the type Cp*Ru(μ-SR)$_n$RuCp* (R = alkyl, aryl; n = 2, 3) have been reported by Hidai for Ru(III)/Ru(III), Ru(II)/Ru(III), and Ru(II)/Ru(II) systems, together with reports of their catalytic and transformation capabilities.[1a,c,6] In comparison, the dithiolate monothioether tpdt ligand in **3**−**5** provides a bridging mode distinctly different from that of monofunctional SR$^-$ ligands. Therefore, it would be interesting to investigate the likely occurrence of a variation of bonding modes of this trisulfur ligand. In this connection, we have studied further the reactions of **2** with other Ru(II) systems, viz. $[Ru(COD)Cl_2]_n$ and $(PPh_3)_3RuCl_2$, and additionally the reactions of the Ru^{II}(tpdt) complex **1** with both a Ru(III) and a Ru(II) system, viz. **2A** and $[Ru(COD)Cl_2]_n$, respectively. It will be seen that, in addition to dinuclear complexes, the reactions give rise to trinuclear Ru complexes containing tpdt in a new μ_3-1κ^3SSS':2κS:3κS-bonding mode or with the metal centers in a near-linear arrangement, multiply bridged by thiolate sulfur atoms and in some cases by an additional M−M bond. There are several examples of chloro-bridged linear triruthenium complexes of the type **B**, reported by Cotton,[7] but thiolate examples are rare.

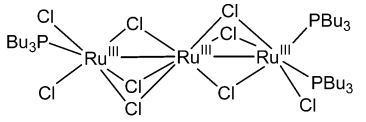

B

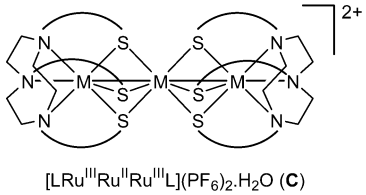

$[LRu^{III}Ru^{II}Ru^{III}L](PF_6)_2.H_2O$ (**C**)

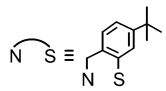

and L = 1,4,7-tris(4-tert-butyl-2-mercaptobenzyl)-1,4,7-triazacyclononane

To our knowledge, Wieghardt had reported the only example (**C**) of such a complex.[8] This paper describes the synthesis, structures, and electrochemistry of the new complexes obtained.

Experimental Section

General Procedures. All reactions were carried out using conventional Schlenk techniques under an atmosphere of nitrogen or under argon in a M. Braun Labmaster 130 inert gas system. NMR spectra were measured on a Bruker 300

(4) Shin, R. Y. C.; Bennett, M. A.; Goh, L. Y.; Chen, W.; Hockless, D. C. R.; Leong, W. K.; Mashima, K.; Willis, A. C. *Inorg. Chem.* **2003**, *42*, 96.

(5) Goh, L. Y.; Teo, M. E.; Khoo, S. B.; Leong, W. K.; Vittal, J. J. *J. Organomet. Chem.* **2002**, *664*, 161.

(6) See for instance: (a) Hidai, M.; Mizobi, Y.; Matsuzaka, H. *J. Organomet. Chem.* **1994**, *473*, 1 (review), and references therein. (b) Nishibayashi, Y.; Onodera, G.; Inada, Y.; Hidai, M.; Uemura, S. *Organometallics* **2003**, *22*, 873. (c) Qu, J.-P.; Masui, D.; Ishii, Y.; Hidai, M. *Chem. Lett.* **1998**, 1003. (d) Takagi, F.; Seino, H.; Hidai, M.; Mizobe, Y. *Organometallics* **2003**, *22*, 1065. (e) Matsuzaka, H.; Hirayama, Y.; Nishio, M.; Mizobe, Y.; Hidai, M. *Organometallics* **1993**, *12*, 36. (f) Matsuzaka, H.; Mizobe, Y.; Nishio, M.; Hidai, M. *J. Chem. Soc., Chem. Commun.* **1991**, 1011.

(7) (a) Bino, A.; Cotton, F. A. *J. Am. Chem. Soc.* **1980**, *102*, 608. (b) Bursten, B. E.; Cotton, F. A.; Fang, A.; *Inorg. Chem.* **1983**, *22*, 2127. (c) Cotton, F. A.; Matusk, M.; Torralba, R. C. *Inorg. Chem.* **1989**, *28*, 1516.

(8) Albela, B.; Bothe, E.; Brosch, O.; Mochizuki, K.; Weyhermuller, T.; Wieghardt, K. *Inorg. Chem.* **1999**, *38*, 5131.

MHz FT NMR spectrometer (^{1}H at 300.14 MHz and ^{13}C at 75.43 MHz); ^{1}H and ^{13}C chemical shifts were referenced to residual solvent in the deuterio solvents $CDCl_3$, CD_2Cl_2, and CD_3CN. Coupling constants (J) are in Hz. IR spectra were measured in KBr pellets in the range 4000−400 cm^{-1} on a BioRad FTS-165 FTIR instrument. FAB and ESI mass spectra were obtained on Finnigan Mat 95XL-T and MATLCQ spectrometers, respectively. Elemental analyses were performed by the microanalytical laboratory in house. Conductivity measurements were carried out at 300 K on 5×10^{-5}−7×10^{-3} M solution in acetonitrile, using a Kyoto Electronics CM-115 conductivity bridge. Cyclic voltammetric and controlled-potential electrolysis experiments were conducted with a PAR Model 273A potentiostat/galvanostat controlled through a PC with standard PAR electrochemical software. Cyclic voltammograms were performed using a 1.0 mm diameter glassy-carbon (GC) working electrode in conjunction with a Pt-wire auxiliary electrode and an Ag-wire reference electrode. EPR measurements were made on a Bruker ESP 300e spectrometer. The compounds [(HMB)Ru(tpdt)] (**1**),[4] [Cp*Ru(tpdt)] (**2**),[5] [(HMB)RuCl$_2$]$_2$ (**1A**),[9] [Cp*RuCl$_2$]$_2$ (**2A**),[10] [Ru(COD)Cl$_2$]$_n$,[11] and (PPh$_3$)$_3$RuCl$_2$[12] were prepared as reported in the literature. CH_3CN was distilled from calcium hydride and MeOH from freshly generated magnesium methoxide before use. All other solvents were distilled from sodium benzophenone ketyl.

Reactions of [(HMB)Ru(tpdt)] (1). (a) With [Cp*RuCl$_2$]$_2$ (2A). Into a stirred red solution of **1** (50 mg, 0.12 mmol) in THF (15 mL) was added **2A** (37 mg, 0.06 mmol). After ca. 10 min at ambient temperature, a homogeneous dark brown solution was obtained, from which a brown precipitate began to separate after ca. 20 min. After 1 h the solids were separated from the supernatant by filtration. The supernatant was evacuated to dryness and the residue extracted with CH_3CN (3×2 mL) to give a dark brown solution, from which the solvent was totally removed and replaced by CD_3CN for a proton NMR spectrum. Black diffraction-quality orthorhombic crystals of [{Ru(μ-1κ^3*SSS*′:2κ^2*SS*-tpdt)Cl$_2$(CH$_3$CN)}Cp*RuCl]·CH$_3$CN (**6**·CH$_3$CN; 5 mg, 7% yield) were formed in the NMR tube after 24 h at room temperature. The precipitated crude solid product was extracted with CH_3CN (3×5 mL) to dissolve a brown complex, leaving insoluble red solids of [{(HMB)Ru(μ_3-1κ^3*SSS*′:2κ*S*:3κ*S*-tpdt)}{Cp*Ru(μ-Cl)}$_2$] (**7**; 15 mg, 13%), which were soluble only in CH_2Cl_2 in which it was found to slowly decompose. Ether diffusion into a dichloromethane solution gave red rectangular needles of **7** after 2 days at −30 °C. The extract was evacuated to dryness and the residue recrystallized in CH_2Cl_2−ether. Fine brown needlelike crystals of [{(HMB)Ru(μ-1κ^3*SSS*′:2κ^2*SS*-tpdt)}RuCl(μ-2κ^3*SSS*′:3κ^2*SS*-tpdt){Cp*RuCl}]Cl (**8**; 33 mg, 54%) were obtained after 2 days at −30 °C.

To a brown solution of **8** (20 mg, 0.02 mmol) in CH_3CN was added NH_4PF_6 (30 mg, 0.18 mmol), and the suspension was stirred for 30 min and then filtered through a disk of Celite (1.5 cm thick) to remove NH_4Cl and excess NH_4PF_6. The deep red filtrate was evacuated to dryness and dissolved in CH_3NO_2. Layering with ether gave black crystals of [{(HMB)Ru(μ-1κ^3*SSS*′:2κ^2*SS*-tpdt)}Ru(μ-2κ^3*SSS*′:3κ^2*SS*-tpdt){Cp*Ru(μ-Cl)}](PF$_6$)$_2$ (**9**; 23 mg, 95% yield) after 24 h at −30 °C.

Data for compound **6** are as follows. ^{1}H NMR (δ; CD_2Cl_2): SC*H*$_2$, unresolved multiplets centered at 3.55 (2H), 3.15 (2H), 2.74 (2H), 2.56 (2H); C*H*$_3$CN, 1.96 (s, 3H); C$_5$*Me*$_5$, 1.60 (s, 15H). ^{13}C NMR (δ, CD_2Cl_2): *C*$_5$Me$_5$, 102.4; S*C*H$_2$, 41.7, 40.6; C$_5$*Me*$_5$, 9.9. IR (ν, cm^{-1}; KBr): 2995 w, 2962 w, 2916 m, 2263 w (C≡N), 2230 w, 2100 w, 2022 w, 1373 vs, 1262 w, 1234 w, 1160 msh, 1099 ssh, 1072 s, 1021 vs, 928 w, 905 w, 803 m, 668 w, 617 w. ESI$^+$ MS: m/z 563 [M − CH$_3$CN − S + H]$^+$. Anal. Found: C, 32.5; H, 4.6; N, 4.7; S, 14.3. Calcd for $C_{16}H_{26}Cl_3NRu_2S_3$·CH$_3$CN: C, 31.9; H, 4.3; N, 4.1; S, 14.2. (A repeat microanalysis was not possible on account of insufficient material due to the low yield. Hence, the proton NMR spectrum is given in Figure S1 in the Supporting Information for support of characterization of bulk material.)

Data for compound **7** are as follows. ^{1}H NMR (δ; CD_2Cl_2): 2(C$_5$*Me*$_5$) + SC*H*$_2$'s, 2.52 (s, $\nu_{1/2}$ ca. 40 Hz, 38H); C$_6$*Me*$_6$, 2.09 (s, 18H). IR (ν, cm^{-1}; KBr): 2963 msh, 2950 msh, 2897 s, 2351 w, 2329 w, 1448 m, 1379 m, 1152 w, 1069 m, 1026 s, 948 w, 918 w, 820 w, 810 w. FAB$^+$ MS: m/z 960 [M − H]$^+$, 687 [M − Cp*RuCl]$^+$, 652 [M − Cp*RuCl$_2$]$^+$. Anal. Found: C, 45.6; H, 5.8; S, 9.7. Calcd for $C_{36}H_{56}Cl_2Ru_3S_3$: C, 45.1; H, 5.9; S, 10.0.

Data for compound **8** are as follows. ^{1}H NMR (δ; CD_3CN): SC*H*$_2$, unresolved multiplets centered at δ 3.41 (2H), 3.10 (1H), 2.88 (5H), 2.72 (1H), 2.01 (3H), 1.87 (4H); C$_6$*Me*$_6$, 2.11 (s, 18H); C$_5$*Me*$_5$, 1.56 (br s, 15H); C*H*$_2$Cl$_2$, 5.44. FAB$^+$ MS: m/z 978 [M − Cl + 2H]$^+$, 941 [M − 2Cl]$^+$, 471 [M − 2Cl]$^{2+}$. Anal. Found: C, 33.7; H, 5.0; S, 15.4. Calcd for $C_{30}H_{49}Cl_3Ru_3S_6$·CH_2Cl_2: C, 34.0; H, 4.7; S, 17.5.

Data for compound **9** are as follows. ^{1}H NMR (δ; CD_3CN): SC*H*$_2$, 3.72−3.64 (8-line m, 2H), 3.13−2.97 (9-line m, 4H), 2.92−2.83 (5-line m, 2H), 2.68−2.55 (7-line m, 4H), 2.36−2.25 (8-line m, 2H), 2.10−2.00 (5-line m, 2H); C$_6$*Me*$_6$, 2.14 (s, 18H); C$_5$*Me*$_5$, 1.84 (s, 15H). ^{13}C NMR (δ; CD_3CN): *C*$_6$Me$_6$, 103.1; *C*$_5$Me$_5$, 96.8; S*C*H$_2$, 41.7, 40.5, 39.5, 32.0; C$_6$*Me*$_6$, 15.6; C$_5$*Me*$_5$, 11.1. IR (ν, cm^{-1}; KBr): 2971 w, 2928 w, 1407 m, 1383 m, 1280 w, 1240 w, 1166 w, 1121 w, 1068 m, 1023 m, 940 wsh, 843 vs (PF_6), 740 w, 673 w, 558 s (PF_6). FAB$^+$ MS: m/z 1087 [M − PF$_6$ + 1]$^+$, 941 [M − 2PF$_6$]$^+$, 913 [M − 2PF$_6$ − 2CH$_2$]$^+$, 750 [M − 2PF$_6$ − 2CH$_2$ − C$_6$Me$_6$]$^+$, 687 [M − 2PF$_6$ − 2CH$_2$ − C$_6$Me$_6$ − 2S]$^+$, 658 [M − 2PF$_6$ − 4CH$_2$ − C$_6$Me$_6$ − 2S]$^+$, 626 [M − 2PF$_6$ − 4CH$_2$ − C$_6$Me$_6$ − 4S]$^+$, 599 [M − 2PF$_6$ − 6CH$_2$ − C$_6$Me$_6$ − 4S]$^+$, 471 [M − 2PF$_6$]$^{2+}$. FAB$^-$ MS: m/z 145 [PF$_6$]$^-$. Anal. Found: C, 29.3; H, 3.9; P, 4.7; S, 15.1. Calcd for $C_{30}H_{49}ClF_{12}P_2Ru_3S_6$: C, 29.3; H, 4.0; P, 5.0; S, 15.6.

(b) With [Ru(COD)Cl$_2$]$_n$. To a suspension of [Ru(COD)Cl$_2$]$_n$ (30 mg, 0.11 mmol, based on monomer) in CH_3CN (5 mL) was added **1** (44.5 mg, 0.11 mmol), and the orange-red solution was heated at 80 °C for 3 h. The solution slowly turned from orange-red to dark brown with precipitation of yellow solids of [(HMB)Ru(μ-1κ^3*SSS*′:2κ^2*SS*-tpdt)Ru(COD)Cl$_2$] (**10**; 22.3 mg, 60% yield). The yellow solids were filtered, washed with 1/4 CH_3CN/ether (3×2 mL), dried in vacuo, and then recrystallized from CH_2Cl_2/hexane.

To a yellow suspension of **10** (10 mg, 0.014 mmol) in CH_3CN was added excess NH_4PF_6 (9 mg, 0.056 mmol) with stirring. After 1 h, the mixture was filtered through Celite to remove NH_4Cl and excess NH_4PF_6. The filtrate was concentrated to ca. 1 mL and ether (4 mL) added. Yellow diffraction-quality crystals of [(HMB)Ru(μ-1κ^3*SSS*′:2κ^2*SS*-tpdt)Ru(COD)(CH$_3$CN)$_2$](PF$_6$)$_2$·3CH$_3$CN (**11**·3CH$_3$CN) were obtained after 3 days at −30 °C.

Data for compound **10** are as follows. ^{1}H NMR (δ; CD_2Cl_2): C*H*$_2$ (COD) + SC*H*$_2$'s, 4.55−4.46 (6-line m, 1H), 4.34−4.24 (6-line m, 1H), 3.36−3.21 (m, 1H), 3.26−3.16 (6-line m, 1H), 3.11−2.98 (10-line m, 2H), 2.91−2.83 (5-line m, 1H), 2.79−2.69 (8-line m, 1H), 2.39−2.18 (9-line m, 3H), 1.87−1.72 (8-line m, 1H), 1.62−1.48 (m, 4H); C*H* (COD), 4.01 (t, J = 7 Hz, 1H), 3.76−3.68 (4-line m, 1H), 3.57 (t, J = 7 Hz, 1H), 3.44 − 3.37 (m, 1H); C$_6$*Me*$_6$, 2.08 (s, 18H). ^{13}C NMR (δ; CD_2Cl_2): *C*$_6$*Me*$_6$, 100.9; *C*H (COD), 90.4, 88.7, 88.6, 79.7; C*H*$_2$ (COD) + SC*H*$_2$'s, 43.5, 43.1, 33.5, 31.9, 30.7, 30.5, 29.9, 28.1; C$_6$*Me*$_6$, 15.5. IR (ν, cm^{-1}; KBr): 2907 vs, 2865 vs, 2822 s, 2635 m, 2341 m, 1626 m, 1429 s, 1384 vs, 1069 s, 1013 vs, 813 m, 733 w, 689 w. ESI$^+$ MS: m/z 625 [M − 2Cl − H]$^+$, 594 [M − 2Cl − S]$^+$, 311 [M − Ru − COD − 2Cl − S$_2$(CH$_2$)$_3$ − 2H]$^+$. Anal. Found: C, 41.3; H, 5.7; S, 13.4. Calcd for $C_{24}H_{38}Cl_2Ru_2S_3$: C, 41.4; H, 5.5; S, 13.8.

Data for compound **11** are as follows. ^{1}H NMR (δ; CD_2Cl_2): C*H*$_2$ (COD) + SC*H*$_2$'s, 3.53−3.44 (7-line m, 1H), 3.37−3.21 (12-

(9) Bennett, M. A.; Huang, T.-N.; Matheson, T. W.; Smith, A. K. *Inorg. Synth.* **1982**, *21*, 74.
(10) Koelle, U.; Kossakowski, J. *Inorg. Synth.* **1992**, *29*, 225.
(11) Kaesz, H. D. *Inorg. Synth.* **1989**, *26*, 253.
(12) Simmons, B. H. *Inorg. Synth.* **1970**, *12*, 238.

line m, 3H), 3.00−2.80 (12-line m, 5H), 2.75−2.61 (9-line m, 2H), 2.37 (c unres m, 3H), 1.86 (c unres m, 2H); C*H* (COD), 4.51 (t, J = 6 Hz, 1H), 4.13−4.05 (4-line m, 1H), 3.93−3.87 (4-line m, 1H), 3.85−3.79 (3-line m, 1H); CH_3CN, 1.95 (s, 6H); C$_6$*Me*$_6$, 2.09 (s, 18H). ^{13}C NMR (δ; CD_2Cl_2): *C*$_6$Me$_6$, 102.2; *C*H (COD): 95.4, 94.4, 92.4, 90.7; CH_2 (COD) + SCH_2's, 42.6, 40.5, 32.6, 32.4, 30.3, 29.9, 28.7, 26.9; C$_6$*Me*$_6$, 15.6; *C*H$_3$CN, 1.9. FAB$^+$ MS: m/z 624 [M − 2PF$_6$ − 2CH$_3$CN]$^+$, 461 [M − 2PF$_6$ − 2CH$_3$CN − C$_6$Me$_6$ − H]$^+$. FAB$^-$ MS, m/z 145 [PF$_6$]$^-$. Anal. Found: C, 33.8; H, 5.1; N, 3.3; S, 10.1. Calcd for $C_{28}H_{44}F_{12}N_2P_2Ru_2S_3$: C, 33.7; H, 4.5; N, 2.8; S, 9.7.

Reactions of [(Cp*)Ru(tpdt)] (2). (a) With [Ru(COD)Cl$_2$]$_n$. To a suspension of [Ru(COD)Cl$_2$]$_n$ (101 mg, 0.36 mmol, based on monomer) in CH$_3$CN (5 mL) was added **2** (279 mg, 0.72 mmol) and the mixture refluxed for 3 h. The mixture slowly changed from dark purple through brown to green. The mixture was filtered through Celite to remove some unreacted starting material. Slow addition of ether (5 mL) into the green solution with stirring gave green solids of [{Cp*Ru(μ-1κ^3*SSS*′:2κ^2*SS*-tpdt)}$_2$RuCl]Cl (**12**; 303 mg, 89% yield).

To a dark green solution of **12** (150 mg, 0.16 mmol) in CH$_3$CN was added excess NH$_4$PF$_6$ (100 mg, 0.63 mmol) with stirring. After 30 min, the mixture was filtered through Celite to remove NH$_4$Cl and excess NH$_4$PF$_6$. The filtrate was concentrated to ca. 3 mL and ether (8 mL) added. Dark green crystals of [{Cp*Ru(μ-1κ^3*SSS*′:2κ^2*SS*-tpdt)}$_2$Ru(CH$_3$CN)](PF$_6$)$_2$·CH$_3$CN (**13**·CH$_3$CN) were obtained after 2 h at −30 °C (176 mg, 92% yield).

(b) With (PPh$_3$)$_3$RuCl$_2$. Into a stirred solution of **2** (24 mg, 0.062 mmol) in MeOH (10 mL) was added (PPh$_3$)$_3$RuCl$_2$ (59 mg, 0.062 mmol). After it was stirred for 2 h at room temperature, the dark green solution was filtered and NH$_4$PF$_6$ (40 mg, 0.24 mmol) was added. After this mixture was stirred for 1 h, the dark green solids that formed were filtered through a glass sinter (porosity no. 4). The solids were extracted with CH$_3$CN (3 × 2 mL) to separate the product from NH$_4$Cl and excess NH$_4$PF$_6$. Addition of ether to the extract gave dark green crystals of **13** (29 mg, 78%) after 1 day at −30 °C.

Data for compound **12** are as follows. ^{1}H NMR (δ; $CDCl_3$): SCH_2, unresolved multiplets centered at δ 3.39 (2H), 3.16 (2H), 2.59 (2H), 2.46 (2H), 2.33 (4H) and 1.65 (4H); C$_5$*Me*$_5$, 1.91 (s, 30H); CH_2Cl$_2$, 5.29. ^{13}C NMR (δ; $CDCl_3$): *C*$_5$*Me*$_5$, 100.3; S*C*H$_2$, 46.8, 42.8, 37.7, 35.4; C$_5$*Me*$_5$, 10.7. IR (ν, cm^{-1}; KBr): 2907 m, 1631 m, 1379 m, 1082 m, 1027 s, 926 w, 803 w. FAB$^+$ MS: m/z 913 [M − Cl − H]$^+$, 877 [M − 2Cl − H]$^+$, 496 [M − 2Cl − C$_5$Me$_5$ − 2Ru − SCH$_2$]$^+$, 388 [M − 2Cl − C$_5$Me$_5$ − (SCH$_2$CH$_2$)$_2$S − 2Ru]$^+$. The conductivity measurement of complex **12** in CH$_3$CN gives the molar conductivity Λ_m = 135.4 Ω^{-1} cm^2 mol^{-1} at 10^{-3} M from the Onsager plot. The molar conductivity falls in the range for a 1:1 electrolyte.[13] Anal. Found: C, 34.8; H, 5.2; S, 19.1. Calcd for $C_{28}H_{46}Cl_2Ru_3S_6$·0.5CH_2Cl_2: C, 34.5; H, 4.7; S, 19.4.

Data for compound **13** are as follows. ^{1}H NMR (δ; CD_2Cl_2): SCH_2, 3.37−3.29 (8-line m, 2H), 3.00−2.94 (5-line m, 2H), 2.88−2.80 (6-line m, 2H), 2.63−2.34 (20-line m, 6H), 1.63−1.54 (5-line m, 2H), 1.45−1.36 (5-line m, 2H); C*H*$_3$CN, 1.97 (s, 3H); C$_5$*Me*$_5$, 1.89 (s, 30H). ^{13}C NMR (δ; CD_2Cl_2): *C*$_5$Me$_5$, 103.2; S*C*H$_2$, 43.4, 39.4, 38.1, 33.4; C$_5$*Me*$_5$, 10.8. IR (ν, cm^{-1}; KBr): 2340 w, 1631 w, 1380 w, 1074 w, 1028 w, 840 s (PF$_6$), 558 m (PF$_6$). FAB$^+$ MS: m/z 879 [M − 2PF$_6$ − CH$_3$CN + H]$^+$, 851 [M − 2PF$_6$ − CH$_3$CN − 2CH$_2$ + H]$^+$, 734 [M − 2PF$_6$ − CH$_3$CN − S − 8CH$_2$]$^+$, 701 [M − 2PF$_6$ − CH$_3$CN − 2S − 8CH$_2$ + H]$^+$. FAB$^-$ MS: m/z 145 [PF$_6$]$^-$. Anal. Found: C, 30.3; H, 4.0; N, 2.0; P, 4.9; S, 15.4. Calcd for $C_{30}H_{49}F_{12}NP_2Ru_3S_6$·CH$_3$CN: C, 30.7; H, 4.2; N, 2.2; P, 5.0; S, 15.4.

Electrochemical Studies. Electrolyzed solutions were prepared in a divided controlled-potential electrolysis cell separated with a porosity no. 5 (1.0−1.7 μm) sintered-glass frit. The working and auxiliary electrodes were identically sized Pt-mesh plates symmetrically arranged with respect to each other with an Ag wire reference electrode (isolated by a salt bridge) positioned to within 5 mm of the surface of the working electrode. The electrolysis cell was jacketed in a glass sleeve and cooled to 233 K using a Lauda variable-temperature methanol circulating bath. The working and auxiliary electrode compartments (ca. 25 mL each) were filled with previously deoxygenated solutions using a vacuum syringe and continually purged with argon during the electrolysis. The number of electrons transferred during the bulk oxidation process was calculated from

$$N = Q/nF \qquad \text{(iv)}$$

where N = number moles of starting compound, Q = charge (coulombs), n = number of electrons, and F is the Faraday constant (96 485 C mol^{-1}).

EPR Experiments. The bottom of the working electrode compartment of the electrolysis cell described above was connected via glass tubing to an evacuated 2 mm diameter cylindrical quartz tube suspended in a dry ice/ethanol bath maintained at 230 K. Opening the tap on the bottom of the electrolysis cell at the completion of the electrolysis allowed the solution to flow rapidly into the quartz tube, which was sealed with a Teflon tap before being further cooled in liquid nitrogen. The EPR cell was then transferred to a Bruker ESP 300e spectrometer employing a TE$_{102}$ cavity with liquid He cooling. EPR simulations were performed using the Bruker computer software WINEPR SimFonia.

Crystal Structure Determinations. The crystals were mounted on glass fibers. X-ray data were collected on a Bruker AXS SMART APEX CCD diffractometer, using Mo Kα radiation (λ = 0.710 73 Å) at 223 K.

The program SMART[14] was used for collecting the intensity data and for the indexing and determination of lattice parameters, SAINT[15] was used for the integration of the intensity of reflections and scaling, SADABS[14] was used for absorption correction, and SHELXTL[16] was used for space group and structure determination and least-squares refinements against F^2. The structures were solved by direct methods to locate the heavy atoms, followed by difference maps for the light nonhydrogen atoms. The hydrogens were placed in calculated positions. A dichloromethane molecule sitting on the mirror plane of **7** was disordered into two positions with occupancies of 50% each. Fluorine atoms of one of the PF$_6^-$ anions of **9** and **11** were disordered into two sets of positions with occupancies of 60% and 40% in **9** and 75% and 25% in **11**. One of the methylene carbons in **11**$^{2+}$ was also disordered into two positions of 80% and 20% occupancy. There are three acetonitrile molecules present as space-filling solvent in this molecule. Crystal data and refinement parameters are given in Table S1 in the Supporting Information.

Results and Discussion

Syntheses and Reaction Pathways. The reaction of [(HMB)Ru^{II}(tpdt)] (**1**) with 0.5 mol equiv of [Cp*Ru^{III}Cl$_2$]$_2$ (**2A**) gives the triruthenium complex [{(HMB)Ru^{II}(μ-1κ^3*SSS*′:2κ^2*SS*-tpdt)}Ru^{III}Cl(μ-2κ^3*SSS*′:3κ^2*SS*-tpdt){Cp*Ru^{III}Cl}](Cl) (**8**) as the major product (54% yield), which undergoes quantitative transformation into [{(HMB)Ru^{II}(μ-1κ^3*SSS*′:2κ^2*SS*-tpdt)}Ru^{III}(μ-2κ^3*SSS*′:3κ^2*SS*-tpdt){Cp*Ru^{III}(μ-Cl)}](PF$_6$)$_2$ (**9**), isolated as a

(13) (a) Geary, W. J. *Coord. Chem. Rev.* **1971**, *7*, 81. (b) Feltham, R. D.; Hayter, R. G. *J. Chem. Soc.* **1964**, 4587. (b) Hayter, R. G.; Humiec, F. S. *Inorg. Chem.* **1963**, *2*, 306.

(14) *SMART & SAINT Software Reference Manuals, Version 5.0*; Bruker AXS: Madison, WI, 1998.

(15) Sheldrick, G. M. SADABS Software for Empirical Absorption Correction; University of Göttingen, Göttingen, Germany, 2000.

(16) *SHELXTL Reference Manual, Version 5.1*; Bruker AXS: Madison, WI, 1998.

Scheme 1

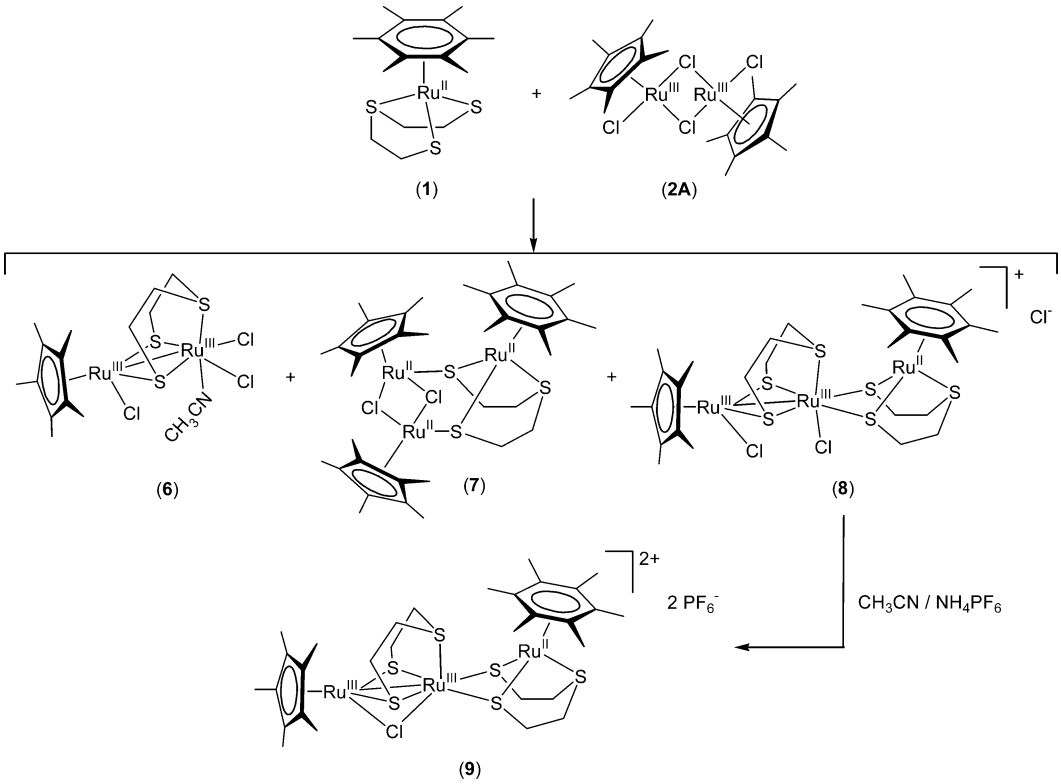

Scheme 2

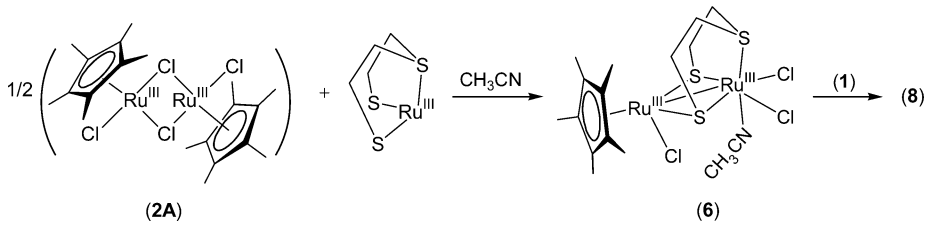

reddish black solid (Scheme 1), together with the red complex [{(HMB)Ru^{II}(μ_3-1κ^3SSS':2κS:3κS-tpdt)}{Cp*Ru^{II}-(μ-Cl)}$_2$] (**7**) in ca. 13% yield and the black dinuclear complex [{Ru^{III}(μ-1κ^3SSS':2κ^2SS-tpdt)Cl_2(CH_3CN)}Cp*-Ru^{III}Cl]·CH_3CN (**6**·CH_3CN) in low yield (7%). **8** is formulated on the basis of its ESI^+ mass spectrum, which shows a peak due to a mother cation associated with two hydrogens. The coordination of these chloro ligands to the Ru centers as shown best satisfies the preference of the Ru centers for a six-coordinate configuration: i.e., neglecting the M−M bond in this case. Treatment with NH_4PF_6 abstracts one of the coordinated chlorides, enabling the second chloro ligand to assume a bridging mode, as shown in the molecular structure of **9**.

The structural analysis of both dinuclear **6** and trinuclear **9** (see below) shows the presence of a Ru^{III}-(κ^3SSS'-tpdt) moiety, which must have originated from **1** via cleavage of the arene ring from its oxidized derivative. The simultaneous formation and isolation of **7** containing the "Ru-reduced" Ru^{II}_2(μ-Cl)$_2$ core of **2A** suggests that the reaction is initiated by a redox process between **1** and **2A,** resulting in oxidation of **1** to Ru^{III} with consequential labilizing of its arene ring, which is then easily cleaved. It is proposed that the resulting highly coordinatively unsaturated and electronically deficient Ru^{III}(κ^3SSS'-tpdt) moiety then inserts into Ru−Cl bonds of a monomeric fragment of **2A** to form **6**. It is conceivable that nucleophilic displacement of a chloro ligand and a ligated CH_3CN molecule in this complex by the thiolate S atoms of **1** forms species **8** (Scheme 2). Indeed, this is confirmed by an NMR experiment, and the fact that it is isolated at all was because of a probable slight deficiency of **1**, thus preventing its total conversion to **8**. A similar nucleophilic displacement in the reduced derivative of **2A** by the thiolate S atoms of the tpdt ligand of **1** generates complex **7**.

The reaction of **1** with 1 mol (monomer) equiv of [Ru^{II}-(COD)Cl_2]$_n$ gives yellow solids of [(HMB)Ru^{II}(μ-1κ^3SSS':2κ^2SS-tpdt)Ru^{II}(COD)Cl_2] (**10**) in 60% yield. After many failed attempts to get a diffraction-quality crystal of **10**, a small sample was treated with NH_4PF_6, whereupon the cationic complex [(HMB)Ru^{II}(μ-1κ^3SSS':2κ^2SS-tpdt)-Ru^{II}(COD)(CH_3CN)$_2$](PF_6)$_2$ (**11**) was obtained (Scheme 3).

The reaction of [Cp*Ru^{III}(tpdt)] (**2**) with [Ru(COD)-Cl_2]$_n$ gives green solids of [{Cp*Ru^{III}(μ-1κ^3SSS':2κ^2SS-tpdt)}$_2$$Ru^{II}$Cl]Cl (**12**) in 89% yield. Treatment of this compound with NH_4PF_6 in CH_3CN results in conversion to [{Cp*Ru^{III}(μ-1κ^3SSS':2κ^2SS-tpdt)}$_2$$Ru^{II}$($CH_3CN$)]($PF_6$)$_2$ (**13**), isolated as dark green crystals. The latter is also

Scheme 3

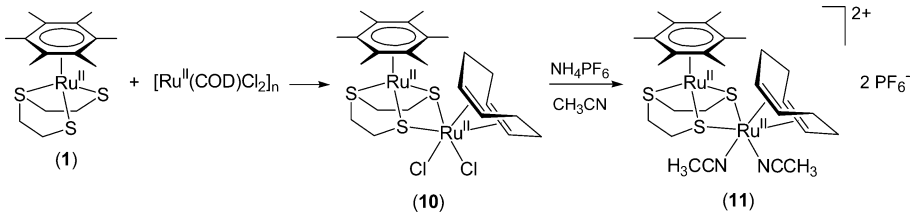

Scheme 4

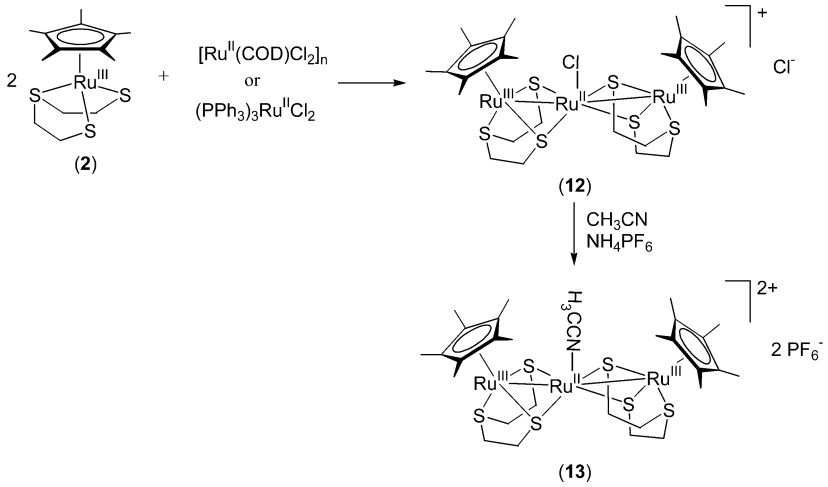

obtained in 78% yield from the reaction of $(PPh_3)_3Ru^{II}Cl_2$ with **2**, followed by metathesis with NH_4PF_6 (Scheme 4).

Crystallographic Studies. The molecular structures of the binuclear complexes [{Ru^{III}(μ-1κ^3SSS':2κ^2SS-tpdt)Cl_2(CH_3CN)}Cp*Ru^{III}Cl] (**6**) and [(HMB)-Ru^{II}(μ-1κ^3SSS':2κ^2SS-tpdt)Ru^{II}(COD)(CH_3CN)$_2$]$^{2+}$ (**11**$^{2+}$) and of the trinuclear complexes [{(HMB)Ru^{II}(μ_3-1κ^3SSS':2κS:3κS-tpdt)}{Cp*Ru^{II}(μ-Cl)}$_2$] (**7**), [{(HMB)Ru^{II}(μ-1κ^3SSS':2κ^2SS-tpdt)}Ru^{III}(μ-2κ^3SSS':3κ^2SS-tpdt)-{Cp*Ru^{III}(μ-Cl)}]$^{2+}$ (**9**$^{2+}$), and [{Cp*Ru^{III}(μ-1κ^3SSS':2κ^2SS-tpdt)}$_2Ru^{II}$(CH_3CN)]$^{2+}$ (**13**$^{2+}$) are shown in Figures 1−5, respectively. Selected bond distances and angles for the five complexes are listed in Table 1.

The molecular structure of **6** possesses a mirror plane of symmetry that contains the Ru(1)−Ru(2), Ru(1)−Cl-(1), and Ru(2)−$NCCH_3$ bonds and bisects the Cp* ring and the Cl(2)−Ru(2)−Cl(2A) angle. The M−M distance of 2.8128(3) Å is significantly shorter than those of **4** (2.8427 Å) and **5** (2.8826 Å). The two bridging thiolate sulfur atoms are almost equidistant from the two Ru atoms (Ru(1)−S(1) = 2.2884(6) Å, Ru(2)−S(1) 2.2863-(6) Å). The Ru(2)−S(2)(thioether) bond distance is 2.2781(8) Å. These Ru−S distances are all shorter than those found in **4** (range 2.2937(9)−2.3197(8) Å) and in **5** (range 2.3134(9)−2.3465(10) Å). Taking into account the M−M bond, the coordination of Ru(1) to a planar η^5-Cp* ring, two thiolate sulfur atoms, and one chloro ligand gives the complex a distorted four-legged pianostool geometry with Ru(2) being seven-coordinate. Ru-(2) is 0.1004 Å above the plane formed by the thiolate sulfurs (S(1) and S(1A)) and the two chloro ligands (Cl-(2) and Cl(2A)) (sum of subtended angles at Ru(2) being 359.57°), while Ru(1) is 0.4410 Å above this extended plane. The Ru(1)−Ru(2) bond forms the backbone of a shallow "wedge" with S(1) and S(1A) (S(1)−Ru(2)−Ru-(1) = S(1A)−Ru(2)−Ru(1) = 52.093°, S(1)−Ru(2)−S(1A) = 102.51(3)°). The thioether sulfur (S(2)) and the acetonitrile ligand may be considered to be occupying pseudoaxial positions at an angle of 169.49(8)°.

The molecular structure of **7** consists of a [(HMB)Ru-(κ^3SSS'-tpdt)] moiety coordinated via its thiolate S atoms to the Ru_2(μ-Cl_2) core in the reduced derivative of **2A**; there thus exists a triruthenium unit with all three metal centers in the +2 oxidation state (as supported by the neutral nature of the molecule), linked by tpdt in a new μ_3-1κ^3SSS':2κS:3κS-bonding mode, and two of the metal centers doubly bridged by chloro ligands. A mirror plane bisects the molecule through Ru(1), Cl(1), and Cl(2). The nonbonding distances between the metal centers are Ru(1)−Ru(2)/Ru(2A) = 4.291 Å and Ru(2)−Ru(2A) = 3.824 Å. The latter distance in the Ru^{III}_2(μ-Cl_2) core of **2A** was reported to be equal to 2.930(1) and 3.752(1) Å in the two "deformational" isomers present in the unit cell of the crystal.[17] The thiolate S atoms of tpdt are slightly closer to Ru(1) (2.379(2) Å) than Ru(2)/Ru(2A) (2.413(2) Å; this compares with the Ru−S distances 2.3396(10), 2.3851-(10), and 2.3807(10) Å in **1**,[4] 2.2937(9)−2.3004(8) Å in **4**, and 2.3151(10)−2.3465(10) Å in **5**.[5] The distances of each Ru center to the bridging chloro atoms are marginally different (2.482(2) and 2.505(2) Å, respectively), both values being significantly longer than the corresponding bond distances (2.36 and 2.46 Å) in the two isomers of **2A**.[17] The angle subtended by the thiolate S atoms at Ru(1) is 93.46(11)°, while the thiolate−Ru−thioether angles are each equal to 86.30(8)°. In the four-membered Ru_2Cl_2 ring, the angle at Ru is 79.05(8)° and those at Cl are 100.78(11)° (Cl(1)) and 99.51(10)° (Cl-

(17) (a) Kölle, U.; Kossakowski, J.; Klaff, N.; Wesemann, L.; Englert, U.; Herberich, G. E. *Angew. Chem., Int. Ed. Engl.* **1991**, *30*, 690. (b) Kolle, U.; Lueken, H.; Handrick, K.; Schilder, H.; Burdett, J. K.; Balleza, S. *J. Am. Chem. Soc.* **1995**, *34*, 6273.

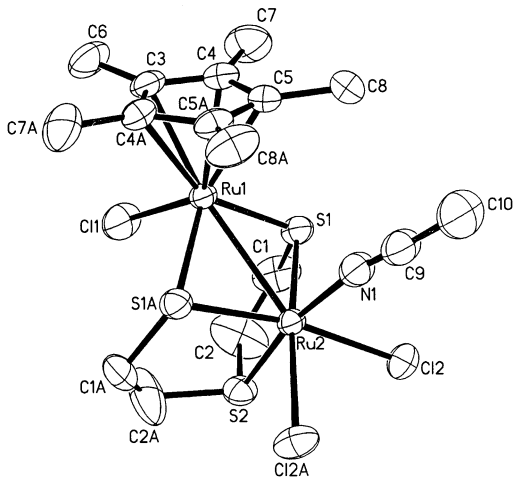

Figure 1. ORTEP plot for the molecular structure of **6.** Thermal ellipsoids are drawn at the 50% probability level.

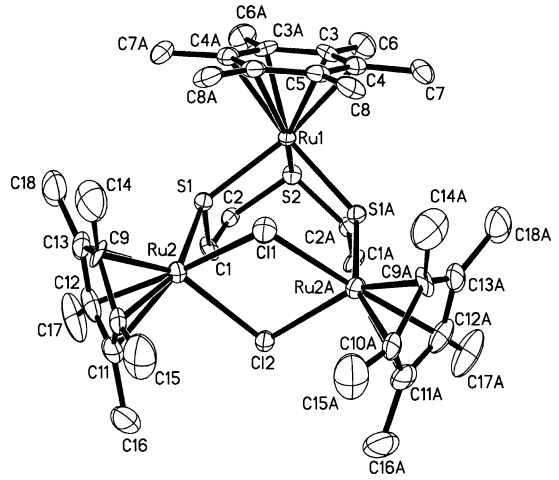

Figure 2. ORTEP plot for the molecular structure of **7.** Thermal ellipsoids are drawn at the 50% probability level.

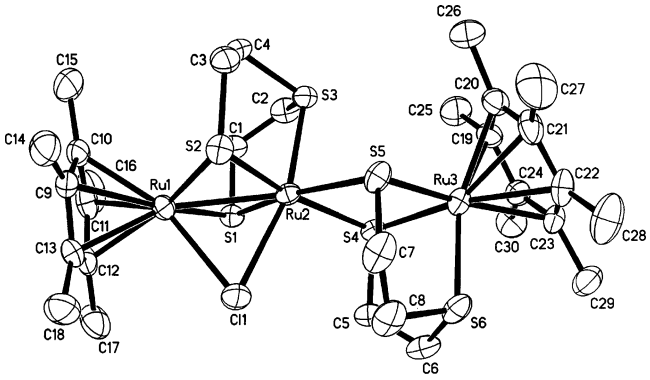

Figure 3. ORTEP plot for the molecular structure of $\mathbf{9}^{2+}$. Thermal ellipsoids are drawn at the 50% probability level.

(2)), compared to 100.24(5) and 76.50(4)° for the Ru−Cl−Ru angles in the isomers of **2A**.[17]

The molecular structure of the PF_6^- salt of complex **9** shows a [(HMB)Ru^{II}(κ^3SSS'-tpdt)] unit coordinated to a diruthenium unit similar to that of **6**, wherein coordinated CH_3CN and a chloro ligand have been replaced by two thiolate ligands, viz. S(4) and S(5) of [(HMB)Ru^{II}(κ^3SSS'-tpdt)], and the second terminal chloro ligand has taken a bridging mode (Cl(1) in **9**), at distances of 2.5201(16) and 2.4765(16) Å from Ru(1) and

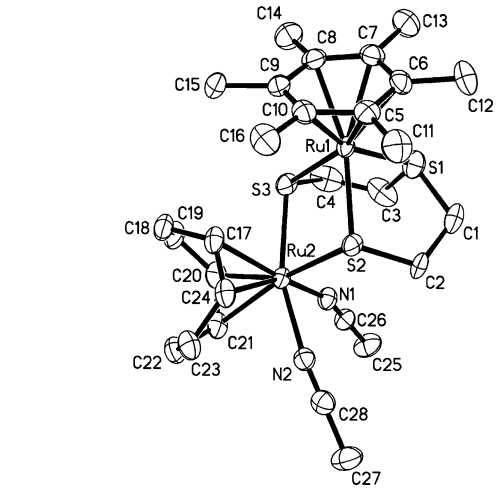

Figure 4. ORTEP plot for the molecular structure of $\mathbf{11}^{2+}$. Thermal ellipsoids are drawn at the 50% probability level.

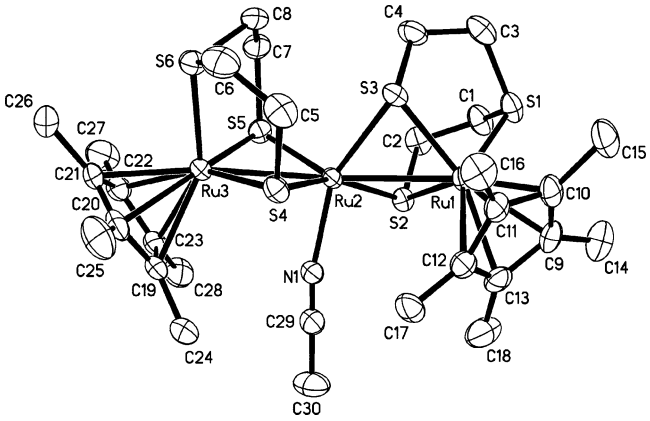

Figure 5. ORTEP plot for the molecular structure of $\mathbf{13}^{2+}$. Thermal ellipsoids are drawn at the 50% probability level.

Ru(2), respectively: i.e., longer than the Ru−μ-Cl bonds in the isomers of **2A**.[17] This has resulted in shortening of the Ru(1)−Ru(2) bond distance from 2.8128(3) Å in **6** to 2.6525(7) Å in **9**. The central ruthenium atom Ru(2) remains in an irregular seven-coordinate environment. On a plane defined by the thiolate ligands, S(1), S(2), S(4), and S(5), Ru(1) and Ru(2) are located 0.6903 and 0.0238 Å, respectively, above the plane, while Ru(3) is located 0.3269 Å below it. The thioether S(3) and Cl(1) ligands may be considered to be in pseudoaxial juxtaposition with respect to each other at Ru(2) (S(3)−Ru(2)−Cl(1) = 163.49(6)°). The distances of Ru(2) to S(1), S(2), and S(3) range from 2.2717(15) to 2.2921(15) Å, while those of Ru(3) to S(4), S(5), and S(6) fall in the range 2.3129(17)−2.3588(15) Å, closer to the range in **1**, as noted above.[4] The donor bonds Ru(1)−S(1) (2.3173(15) Å) and Ru(1)−S(2) (2.3232(15) Å) occur between these two ranges of values. The Ru(2)···Ru(3) nonbonding distance is 3.6475 Å. The Ru(1)−Ru(2)···Ru(3) array is slightly off-linear (the angle at Ru(2) being 170.96°). The dicationic nature of the complex is consistent with oxidation states (III, III, II) for this 54e^- species, with each Ru center bearing 18e^-; the set of oxidation states may be deduced from the origin of the Ru centers: viz., Ru(1) from **2A**, a Ru(III) complex, the central Ru(2) from an oxidized derivative of **1**, and terminal Ru(3) from **1**, a Ru(II) complex.

Table 1. Selected Bond Lengths (Å) and Angles (deg)

Compound **6**[a]

Ru(1)−S(1)	2.2884(6)	Ru(2)−S(1)	2.2863(6)	Ru(2)−Cl(2)	2.4351(6)	Ru(2)−N(1)	2.071(3)
Ru(1)−S(1A)	2.2884(6)	Ru(2)−S(1A)	2.2863(6)	Ru(2)−Cl(2A)	2.4351(6)	Ru(1)−Ru(2)	2.8128(3)
Ru(1)−Cl(1)	2.4195(9)	Ru(2)−S(2)	2.2781(8)				
Cl(1)−Ru(1)−S(1)	95.19(2)	S(1)−Ru(2)−S(1A)	102.51(3)	Cl(2)−Ru(2)−Cl(2A)	86.24(3)	Cl(2)−Ru(2)−S(1)	85.41(2)
Cl(1)−Ru(1)−S(1A)	95.19(2)	S(1)−Ru(2)−S(2)	89.28(2)	Cl(2)−Ru(2)−N(1)	86.79(6)	Cl(2A)−Ru(2)−N(1)	86.79(6)
S(1)−Ru(1)−S(1A)	102.38(3)	S(1A)−Ru(2)−S(2)	89.28(2)				

Compound **7**[a]

Ru(1)−S(1)	2.379(2)	Ru(1)···Ru(2)	4.291	Ru(2)−S(1A)	2.413(2)	Ru(2A)−Cl(1)	2.482(2)
Ru(1)−S(1A)	2.379(2)	Ru(1)···Ru(2A)	4.291	Ru(2)−Cl(1)	2.482(2)	Ru(2A)−Cl(2)	2.505(2)
Ru(1)−S(2)	2.304(3)	Ru(2)−S(1)	2.413(2)	Ru(2)−Cl(2)	2.505(2)	Ru(2)···Ru(2A)	3.824
S(1)−Ru(1)−S(1A)	93.46(11)	S(1)−Ru(2)−Cl(1)	92.18(9)	S(1A)−Ru(2A)−Cl(1)	92.18(9)	Ru(2)−Cl(1)−Ru(2A)	100.78(11)
S(1)−Ru(1)−S(2)	86.30(8)	S(1)−Ru(2)−Cl(2)	90.73(9)	S(1A)−Ru(2A)−Cl(2)	90.73(9)	Ru(2)−Cl(2)−Ru(2A)	99.51(10)
S(1A)−Ru(1)−S(2)	86.30(8)	Cl(1)−Ru(2)−Cl(2)	79.05(8)	Cl(1)−Ru(2A)−Cl(2)	79.05(8)		

Compound **9**$^{2+}$

Ru(1)−S(1)	2.3173(15)	Ru(2)−S(2)	2.2833(15)	Ru(2)−Cl(1)	2.4765(16)	Ru(3)−S(5)	2.3588(15)
Ru(1)−S(2)	2.3232(15)	Ru(2)−S(3)	2.2717(15)	Ru(2)−Ru(1)	2.6525(7)	Ru(3)−S(6)	2.3129(17)
Ru(1)−Cl(1)	2.5201(16)	Ru(2)−S(4)	2.4324(15)	Ru(3)−S(4)	2.3556(15)	Ru(2)···Ru(3)	3.648
Ru(2)−S(1)	2.2921(15)	Ru(2)−S(5)	2.4196(16)				
S(1)−Ru(1)−S(2)	105.65(5)	S(2)−Ru(2)−S(5)	86.99(5)	S(5)−Ru(2)−Cl(1)	103.03(6)	S(3)−Ru(2)−Cl(1)	163.49(6)
S(1)−Ru(1)−Cl(1)	79.77(5)	S(4)−Ru(2)−S(5)	78.74(5)	S(1)−Ru(2)−S(3)	89.43(5)	S(4)−Ru(3)−S(5)	81.52(5)
S(2)−Ru(1)−Cl(1)	78.81(6)	S(1)−Ru(2)−Cl(1)	81.19(5)	S(2)−Ru(2)−S(3)	89.63(6)	S(4)−Ru(3)−S(6)	85.50(6)
S(1)−Ru(2)−S(2)	107.83(6)	S(2)−Ru(2)−Cl(1)	80.47(6)	S(4)−Ru(2)−S(3)	89.05(5)	S(5)−Ru(3)−S(6)	86.93(6)
S(1)−Ru(2)−S(4)	86.41(5)	S(4)−Ru(2)−Cl(1)	103.77(5)	S(5)−Ru(2)−S(3)	89.50(6)	Ru(1)−Ru(2)···Ru(3)	170.96

Compound **11**$^{2+}$

Ru(1)−S(1)	2.2967(8)	Ru(2)−S(2)	2.4244(7)	C(17)−C(18)	1.524(4)	C(21)−C(22)	1.523(4)
Ru(1)−S(2)	2.3757(7)	Ru(2)−S(3)	2.4010(8)	C(18)−C(19)	1.540(4)	C(22)−C(23)	1.540(4)
Ru(1)−S(3)	2.3509(7)	Ru(2)−N(1)	2.075(2)	C(19)−C(20)	1.515(4)	C(23)−C(24)	1.512(4)
Ru(1)···Ru(2)	3.667	Ru(2)−N(2)	2.101(2)	C(20)−C(21)	1.363(4)	C(24)−C(17)	1.375(4)
S(1)−Ru(1)−S(2)	85.83(3)	S(2)−Ru(1)−S(3)	80.24(2)	N(1)−Ru(2)−N(2)	78.75(9)	C(20)−Ru(2)−C(21)	35.54(11)
S(1)−Ru(1)−S(3)	87.82(3)	S(2)−Ru(2)−S(3)	78.28(2)	C(17)−Ru(2)−C(24)	36.14(1)		

Compound **13**$^{2+}$

Ru(1)−S(1)	2.3207(14)	Ru(2)−S(2)	2.3259(13)	Ru(2)−S(5)	2.2910(13)	Ru(3)−S(4)	2.3053(13)
Ru(1)−S(2)	2.3204(13)	Ru(2)−S(3)	2.2987(13)	Ru(2)−N(1)	2.116(4)	Ru(3)−S(5)	2.2788(13)
Ru(1)−S(3)	2.3102(14)	Ru(2)−S(4)	2.3587(13)	Ru(2)−Ru(3)	2.8160(6)	Ru(3)−S(6)	2.3009(14)
Ru(1)−Ru(2)	2.7857(5)						
S(1)−Ru(1)−S(2)	86.14(5)	S(2)−Ru(2)−S(5)	100.91(5)	S(3)−Ru(2)−N(1)	154.02(12)	S(5)−Ru(3)−S(6)	87.54(5)
S(1)−Ru(1)−S(3)	86.46(5)	S(3)−Ru(2)−S(4)	91.51(5)	S(4)−Ru(2)−N(1)	89.77(12)	N(1)−Ru(2)−Ru(1)	102.71(12)
S(2)−Ru(1)−S(3)	90.48(5)	S(3)−Ru(2)−S(5)	105.28(5)	S(5)−Ru(2)−N(1)	99.90(12)	N(1)−Ru(2)−Ru(3)	84.24(12)
S(2)−Ru(2)−S(3)	90.63(5)	S(4)−Ru(2)−S(5)	101.20(5)	S(4)−Ru(3)−S(5)	103.23(5)	Ru(1)−Ru(2)−Ru(3)	162.54(2)
S(2)−Ru(2)−S(4)	156.36(5)	S(2)−Ru(2)−N(1)	78.30(12)	S(4)−Ru(3)−S(6)	87.00(5)		

[a] The molecule possesses a plane of symmetry.

A diffraction-quality crystal of **10** could not be obtained; hence, its structural formulation (see Scheme 3) is based only on its elemental analysis, the absence of a signal due to coordinated CH_3CN in the proton NMR spectrum, and the molecular structure of its CH_3-CN derivative **11.** This reveals a dinuclear unit wherein a μ-1κ^3SSS':2κ^2SS-tpdt ligand bridges (HMB)Ru^{II} and [(η^4-COD)$Ru^{II}(CH_3CN)_2$] moieties. The Ru···Ru nonbonding distance is 3.667 Å. The C═C distances in the COD ligand are 1.363(4) and 1.375(4) Å, compared to 1.512(4)−1.540(4) Å for the other C−C distances in the cyclic diene. The two CH_3CN ligands are in a cis relationship, subtending an angle of 78.75(9)° at Ru(2).

The formulation of **12** with one chloro ligand is based on its conductivity characteristics and microanalytical and mass spectral data and is further supported by the X-ray diffraction analysis of the PF_6^- salt of its chloro-substituted CH_3CN derivative, the trinuclear complex **13**. The molecule of this contains the central ruthenium atom Ru(2) coordinated to a CH_3CN molecule and sandwiched between two [Cp*Ru^{III}(κ^3SSS'-tpdt)] groups, to which it is bridged via two thiolate S atoms of the tpdt ligands and M−M bonds (Ru(1)−Ru(2) = 2.7857(5) Å and Ru(2)−Ru(3) = 2.8160(6) Å); the presence of two metal−metal bonds creates a trimetallic array with an Ru(1)−Ru(2)−Ru(3) angle equal to 162.54(2)°. All three metal centers are formally seven-coordinate. The distances of Ru(3) to the thiolate sulfurs of tpdt are very close to those in **4**; similar distances of Ru(1) are significantly longer, as seen in Table 1.

Spectral Characteristics. The proton NMR spectrum of **6** in CD_2Cl_2 shows resonances at δ 1.60 for Cp* and multiplets at δ 2.56−3.55 for the SCH_2 groups, with corresponding ^{13}C resonances at δ 9.9 and δ 40.6−40.7, respectively, and at δ 102.4 for the Cp* ring carbons. Both Ru(1) and Ru(2) possess odd-valence-electron counts (19e$^-$ and 17e$^-$, respectively). The observed diamagnetism indicates effective coupling of the odd electrons, facilitated by the presence of a M−M bond.

The proton NMR spectrum of **7** in CD_2Cl_2 shows a broad singlet at δ 2.52, assignable to the protons of two Cp* rings and the SCH_2 groups on the basis of its intensity relative to the C_6Me_6 resonance at δ 2.09. The

highest fragment in the FAB^+ MS shows the loss of a hydrogen from the mother ion.

The proton NMR spectrum of **8** in CD_3CN possesses singlets at δ 2.11 and 1.56 for the Me substituents on the arene and Cp* rings, respectively, and six sets of unresolved multiplets at δ 1.87−3.41 for the SCH_2 protons. Lattice CH_2Cl_2 is seen at δ 5.44. The highest peak in the FAB^+ MS conforms to the mother cation associated with two hydrogens.

The proton NMR spectra of **9** in CD_3CN shows methyl singlets at δ 1.84 and 2.14 for the Cp* and C_6Me_6 protons, respectively, and six sets of well-defined multiplets at δ 2.00−3.72 (detailed in the Experimental Section) for the SCH_2 groups. The ^{13}C NMR spectrum shows resonances at δ 11.1 and 15.6 for the methyl carbon atoms of the Cp* and C_6Me_6 ligands, with corresponding ring carbons at δ 96.8 and 103.1 and four signals at δ 32.0−41.7 for the SCH_2.groups. The FAB^+ MS shows the mother ion at *m*/*z* 941.

The proton NMR spectrum of **10** in CD_2Cl_2 shows a singlet at δ 2.08 for the protons of C_6Me_6, multiplets centered at δ 1.55, 1.79, 2.25, 2.75, 2.86, 3.06, 3.22, 3.34, 4.29, and 4.50 for the CH_2 protons of the sulfide ligand and of cycloocta-1,5-diene (COD), and multiplets centered at δ 3.39, 3.57, 3.71, and 4.01 for the CH protons of COD. The ^{13}C NMR spectrum shows peaks at δ 15.5 and 100.9 for the methyl and ring carbon atoms of the C_6Me_6 ligand, peaks at δ 28.1, 29.9, 30.5, 30.7, 31.9, 33.5, 43.1, and 43.5 for SCH_2 carbons and CH_2 carbons of COD, and peaks at δ 79.7, 88.6, 88.7, and 90.4 for the CH carbons of COD. The highest mass fragment in the ESI^+ MS indicates loss of two chloro ligands and a hydrogen from the mother ion, followed by further loss of S (*m*/*z* 594). These data support the formulation of **10,** with both $18e^-$ ruthenium centers in the +2 oxidation state, as presented in Scheme 3. The proton NMR spectrum of **11** in CD_2Cl_2 shows singlets at δ 2.09 and 1.95 for C_6Me_6 and coordinated CH_3CN, respectively, multiplets centered at δ 1.86, 2.37, 2.66, 2.87, 3.30, and 3.49 and for SCH_2's and CH_2 of COD, and multiplets centered at δ 3.82, 3.89, 4.08, and 4.51 for CH protons of COD. The ^{13}C NMR spectrum shows peaks at δ 15.6 and 102.2 for the methyl and ring carbon atoms of the C_6Me_6 ligand, respectively, a peak at δ 1.9 for the methyl carbon of CH_3CN, peaks at δ 26.9, 28.7, 29.9, 30.3, 32.4, 32.6, 40.5, and 42.6 for SCH_2 carbon atoms and CH_2 carbon atoms of COD, and peaks at δ 90.7, 92.4, 94.4, and 95.4 for the CH carbons of COD.

The proton NMR of **12** in $CDCl_3$ shows a single peak for the methyl protons of the two Cp* rings at δ 1.91, six sets of unresolved multiplets for the SCH_2 protons at δ 1.65−3.39, and lattice CH_2Cl_2 at δ 5.29. The ^{13}C NMR spectrum exhibits δ 10.7 and 100.3 for the Cp* methyl and ring carbons and δ 35.4, 37.7, 42.8, and 46.8 for the SCH_2 carbons. The FAB^+ mass spectrum shows loss of a hydrogen from the mother ion at *m*/*z* 913 (M^+) with subsequent loss of Cl (*m*/*z* 877) before further fragmentation. The conductivity measurement of complex **12** in CH_3CN gives the molar conductivity Λ_m = 135.4 Ω^{-1} cm^2 mol^{-1} at 10^{-3} M from the Onsager plot, consistent with a 1:1 electrolyte.[13] This supports the set of oxidation states (III, II, III) for the Ru centers, each bearing $18e^-$ in the $54e^-$ monocationic species **12** and dicationic species **13**.

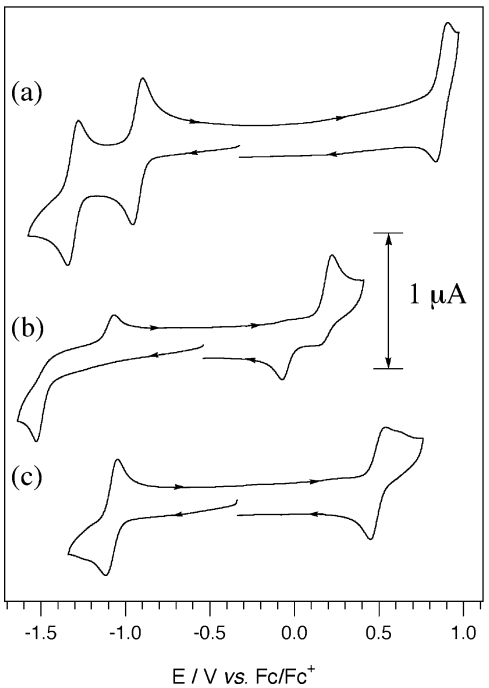

Figure 6. Cyclic voltammograms performed at a 1 mm diameter planar GC electrode in CH_2Cl_2 (0.5 M Bu_4NPF_6) at −40 °C at a scan rate of 100 mV s^{-1} for 0.5 mM (a) **9**, (b) **12**, and (c) **13**.

The proton NMR spectrum of **13** in CD_2Cl_2 shows six sets of resolved multiplets at δ 1.36−3.37 for SCH_2's and singlets at δ 1.97 and 1.89 for coordinated CH_3CN and Cp*, respectively. The corresponding ^{13}C NMR signals are seen at $\delta(SCH_2)$ 33.4, 38.1, 39.4, and 43.4 and $\delta(C_5Me_5)$ 10.8 and 103.2. The highest peak in the FAB^+ MS shows the mother cation with loss of CH_3CN together with association with a hydrogen.

Electrochemical and EPR Studies. Cyclic voltammograms (CV's) of 0.5 mM solutions of **9**, **12**, and **13** in CH_2Cl_2 at a glassy-carbon (GC) electrode are displayed in Figure 6. To improve the stability of the reduced and oxidized states, all voltammetric experiments were conducted at low temperatures (typically −40 °C). Cyclic voltammetry of a solution of **9** displayed two well-defined chemically reversible reduction processes and one chemically reversible oxidation process (Figure 6a) at a scan rate of 100 mV s^{-1}. CV's obtained of solutions of **9** also showed a second oxidation process with a current magnitude similar to that of the first oxidation process (indicating that the same number of electrons were transferred) at more positive potentials (E_p = 1.095, not shown in the CV) that showed no reverse peak when the scan direction was reversed, suggesting chemical instability of the doubly oxidized species.

CV's obtained of solutions of **12** displayed one reduction and one oxidation process (Figure 6b). The reduction was chemically irreversible, but the oxidation showed a small reduction peak (E_p = 0.18 V) on reversal, indicating partial reversibility ($i_{p,c}/i_{p,a} \approx 0.3$). Further, additional processes that appeared on the reverse scans of the main oxidation and reduction processes for **12** at approximately −1.1 and −0.1 V (Figure 6b) are likely to be associated with decomposition products, due to the formation of unstable species following the principal electron-transfer steps.

Table 2. Cyclic Voltammetric Data

	redn processes[a]				oxidn processes[a]			
compd	E_p^{red}/ V[b]	E_p^{ox}/ V[c]	$E^r_{1/2}$/ V[d]	ΔE/ mV[e]	E_p^{ox}/ V[c]	E_p^{red}/ V[b]	$E^r_{1/2}$/ V[d]	ΔE/ mV[e]
9	−0.996	−0.934	−0.965	62	0.942	0.870	0.906	72
	−1.396	−1.328	−1.362	68	1.095			
12	−1.528				0.222			
13	−1.118	−1.046	−1.082	72	0.538	0.448	0.494	90
	−1.876				0.970			

[a] Obtained at a scan rate of 100 mV s^{-1} at a 1 mm diameter glassy-carbon electrode at −40 °C in CH_2Cl_2 with 0.5 M Bu_4NPF_6 as the supporting electrolyte. All potentials are relative to the ferrocene/ferrocenium redox couple. [b] E_p^{red} = reductive peak potential. [c] E_p^{ox} = oxidative peak potential. [d] $E^r_{1/2} = (E_p^{red} + E_p^{ox})/2$. [e] $\Delta E = |E_p^{ox} - E_p^{red}|$.

CV's of solutions of **13** showed one chemically reversible oxidation process and one chemically reversible reduction process (Figure 6c). An additional reduction and oxidation process was present, each with the same current magnitude as the first processes, at more negative and more positive potentials, respectively ($E_{p,c}$ = −1.876, $E_{p,a}$ = 0.970; not shown in the CV), that indicated chemical instability of the doubly reduced/oxidized species.

Table 2 lists the reversible reduction potentials ($E^r_{1/2}$) that were calculated from cyclic voltammetry data under conditions where the ratio of the oxidative (i_p^{ox}) to reductive (i_p^{red}) peak currents was equal to unity and using the relationship

$$E^r_{1/2} = (E_p^{ox} + E_p^{red})/2 \qquad \text{(v)}$$

where E_p^{ox} and E_p^{red} are the anodic and cathodic peak potentials, respectively. In situations where no reverse peak was observed (such as for **12**), only the peak potential is given. In most instances where the E_p^{ox} and E_p^{red} peak separation (ΔE) could be measured, the values obtained were close to those expected for a one-electron-transfer step (Table 2). By assuming that the diffusion coefficients for **9**, **13**, and **12** are all very similar, and by comparing the anodic and cathodic peak currents shown in Figure 6, it is reasonable to expect that the principal processes all occur by the same number of electrons (i.e. n = 1).

Additional data relating to the number of electrons transferred during the oxidation/reduction processes came from coulometry experiments at low temperature (see the Experimental Section). Coulometry experiments were conducted on the two one-electron-reduction processes and first oxidation process of **9**, and the first reduction process of **13** and **12**. In all cases the number of electrons transferred was calculated to be 1.0 ± 0.1, which is in good agreement with the shorter time-scale cyclic voltammetric experiments.

For **9**, the species produced during the first (least negative) reduction was found to be stable for relatively long periods of time in deoxygenated solutions at low temperature ($T \leq$ −40 °C). Considering that in its original state, **9** is diamagnetic, it was thought that the one-electron reduction would lead to a low-spin paramagnetic species, and EPR experiments were conducted to confirm this hypothesis (Figure 7). The rhombic shaped EPR spectrum may be interpreted[18] to indicate that the unpaired electron is principally located on

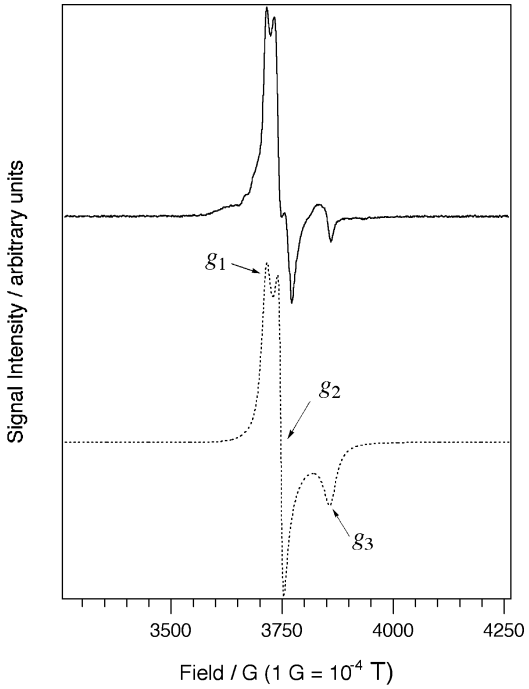

Figure 7. (a) First-derivative X-band EPR spectrum of 0.5 mM [**9**]$^-$ that was obtained by one-electron bulk electrochemical reduction of **9** in CH_2Cl_2 (0.5 M Bu_4NPF_6). Conditions EPR modulation amplitude, 0.5 mT; time constant, 0.16 s; sweep time, 160 s; microwave frequency, 9.436 474 GHz; microwave power, 0.63 μW; T = 6 K. (b) Simulated spectra with 100% Gaussian line shape: g_1 = 2.035 (ΔH_{pp} = 1.5 mT); g_2 = 2.015 (ΔH_{pp} = 0.8 mT); g_3 = 1.950 (ΔH_{pp} = 2.0 mT).

ruthenium in an unsymmetrical environment. A one-electron reduction would lead formally to a complex with one Ru^{III} (d^5) and two Ru^{II} (d^6) atoms. The diamagnetism of **9** containing two Ru^{III} atoms can be explained if the unpaired electrons on the two Ru^{III} ions reside in a shared molecular orbital. A simulation could be approximately matched to the experimental data (Figure 7), although it appears that the experimental spectrum is additionally complicated by unresolved hyperfine coupling, possibly to Cl^- or even aromatic protons. Electrochemical and EPR spectroscopic experiments showed that the one-electron-reduced form of **9** decomposed within 2−3 min of warming to room temperature.

The poor stabilities of the species formed during the main redox processes of **12**, under the present experimental conditions, are attributed to the lability of the Ru−Cl bond, leading to irreversible bond cleavage after the electron-transfer process. This is supported by the observation of loss of Cl^- during PF_6^- exchange and replacement of the Cl^- ligand by a solvent CH_3CN molecule. It is also interesting to compare the peak potentials for the oxidation and reduction of **12** and **13** (as a first approximation only, since processes of **12** are irreversible). These two complexes differ only in whether a Cl^- or CH_3CN ligand is attached to the central Ru. However, this resulted in a large difference in the oxidation peak potentials: 0.222 V for **12** but 0.538 V for **13** (Table 2). This reflected the overall charge environment of +1 for **12** and +2 for **13**, as well as greater electron-donating capability of the chloro ligand.

(18) Rieger, P. H. *Coord. Chem. Rev.* **1994**, *135/136*, 203.

By the same token, the difference in the reduction peak potentials (Table 2) is reversed.

As discussed above, solutions of **13** can be electrochemically reduced and oxidized in one-electron chemically reversible steps. Although single-crystal X-ray data indicated that **13** is slightly dissymmetric in the solid state, as required by the crystal packing, the solution-phase NMR data showed that **13** is symmetrical about the central Ru, and this is taken to be the case in electrochemical experiments. The oxidation states of the Ru_3 metal centers in **13** are $[III, II, III]^{2+}$. Thus, it is reasonable to deduce that the first reversible $1e^-$ reduction occurs with the electron being shared between the (equivalent) terminal Ru ions, giving $[II, II, III]^+ \leftrightarrow [III, II, II]^+$. The reversible $1e^-$ oxidation of **13** most likely gives $[III, III, III]^{3+}$. These redox processes are summarized as

$$[II, II, III]^+ \xleftarrow[E^{\circ\prime} = -1.082\ V]{+e^-} [III, II, III]^{2+} \xrightarrow[E^{\circ\prime} = 0.494\ V]{-e^-} [III, III, III]^{3+}$$

The second one-electron-reduction process of **13** occurs at a substantially more negative potential, although the species that is produced is chemically unstable, with only a small reverse oxidation peak being detected during CV experiments, even at low temperatures (Table 2). Mixed-valence multinuclear complexes, in particular the symmetrical Creutz−Taube-type ions, are of interest, both in theory and in practical applications.[19−21] For symmetrical compounds with more than one redox center, the separation in the electron-transfer steps can be used to determine the comproportionation constant (K_c) that is a measure of the degree of interaction between the metal centers.

$$K_c = \exp[(E_1^\circ - E_2^\circ)F/RT] \qquad \text{(vi)}$$

For compound **13**, the difference in potential between the first and second reduction processes ($E_1^\circ - E_2^\circ$) is ~0.75 V, which leads to a very high value of K_c of 10^{14} for the equilibrium

$$[Ru-Ru-Ru]^{2+} + [Ru-Ru-Ru]^0 \leftrightarrow 2[Ru-Ru-Ru]^+ \qquad \text{(vii)}$$

Values of $K_c > 10^6$ are considered to be indicative of a class III system (extensive delocalization) according to the Robin−Day scheme;[22] hence, the redox properties must be considered in terms of a shared molecular orbital. Valence delocalization is expected between the terminal and central Ru ions of compound **13** due to the presence of Ru−S−Ru mixed-valence centers, arising from back-bonding and electron conduction through the sulfide linkages and the M−M bonds.

9 has oxidation states for Ru of $[III, III, II]^{2+}$. The major difference between **9** and **12**, **13** is that only one of the terminal Ru is bonded to the central Ru; thus, **9** has no 2-fold symmetry through the central Ru ion, whereas in **12** and **13**, both terminal Ru centers are bonded to the central Ru in the same way. Qualitatively, an inspection of the environments of the Ru ions suggests that the first electron transfer to the central Ru(III) (eq viii) is more favorable because of the existence of more sulfide linkages, i.e.

$$[III-III, II]^{2+} + e^- = [III-II, II]^+ \qquad E^{\circ\prime} = -0.965\ V \qquad \text{(viii)}$$

This is in agreement with the inference from EPR data, which indicated that the unpaired electron is located predominantly on a Ru atom in an unsymmetrical environment. Therefore, the second reversible $1e^-$ reduction may occur at the terminal Ru(III) center (eq ix)

$$[III-II, II]^+ + e^- = [II-II, II]^0 \qquad E^{\circ\prime} = -1.362\ V \qquad \text{(ix)}$$

and the reversible oxidation step is illustrated in eq x.

$$[III-III, II]^{2+} = [III-III, III]^{3+} + e^- \qquad E^{\circ\prime} = 0.906\ V \qquad \text{(x)}$$

However, the assignment of the electron-transfer steps for **9** are tentative, since the extent of delocalization is difficult to determine by electrochemical methods for unsymmetrical compounds. The high negative potential for the two-electron reduction of $\mathbf{9}^{2+}$ to the neutral complex ($\mathbf{9}^0$) indicates why it is the dication rather than the neutral species [II, II, II] that is isolated as a stable product, since the dication (and probably the monocation) is a sufficiently strong reducing agent to reduce molecular oxygen to the superoxide anion. It is interesting to compare the potentials for the oxidations of **12**, **13**, and **9**, where **12** ($E^{\circ\prime} \approx 0.20$ V) < **13** ($E^{\circ\prime} = 0.494$ V) < **9** ($E^{\circ\prime} = 0.906$ V). The difference between **12** and **13** has been discussed earlier. The much more positive value for **9** arose because the electron was extracted from a terminal Ru(II), in contrast to a central Ru(II) for **12** and **13**. The presence of the Ru−Ru bonding in **9** may enhance valence delocalization in $[III-II, II]^+$.

Conclusions

The thiolate S atoms of $[Cp^*Ru^{III}(\kappa^3SSS'\text{-tpdt})]$ (**2**) act as effective nucleophiles for the displacement of COD or PPh_3 in chloro-containing Ru(II) complexes, giving rise to M−M-bonded near-linear trimetallic complexes. An initial redox reaction between $[(HMB)Ru^{II}(\kappa^3SSS'\text{-tpdt})]$ (**1**), the $(HMB)Ru^{II}$ analogue of **2**, and $[Cp^*Ru^{III}Cl_2]_2$ (**2A**) results in arene cleavage in **1**, and subsequent reactions of a coordinatively unsaturated and electronically deficient $[Ru^{III}(\kappa^3SSS'\text{-tpdt})]$ moiety with **2A** and of the Ru(II) derivative of **2A** with **1** give three new compounds, viz. a dinuclear Ru^{III}_2 species, an almost linear $Ru^{III}_2Ru^{II}$ species, and a Ru^{II}_3 complex with the tpdt ligand in a new μ_3-$1\kappa^3SSS'$:$2\kappa S$:$3\kappa S$-bonding mode.

Cyclic voltammetric and controlled-potential electrolysis experiments have shown that the triruthenium charged complexes could be reduced and oxidized in one and sometimes two successive one-electron steps. Reduction of the symmetrical compounds is likely to

(19) Demadis, K. D.; Hartshorn, C. M.; Myers, T. J. *Chem. Rev.* **2001**, *101*, 2655.
(20) Kaim, W.; Klein, A.; Glockle, M. *Acc. Chem. Res.* **2002**, *33*, 755.
(21) Moreira, I. S.; Lima, J. B.; Franco, D. W. *Coord. Chem. Rev.* **2000**, *196*, 197.
(22) Robin, M. B.; Day, P. *Adv. Inorg. Chem. Radiochem.* **1967**, *10*, 247.

involve delocalization of the unpaired electron between the terminal Ru ions, leading to the Creutz−Taube-type complex [$Ru^{2.5+}$−Ru^{II}−$Ru^{2.5+}$] with electronic conduction through the bridging sulfide linkages and the Ru−Ru bonds.

Acknowledgment. Support from an Academic Research Grant (Grant No. R-143-000-135-112 to L.Y.G.) of the National University of Singapore and a research scholarship to R.Y.C.S. is gratefully acknowledged.

Supporting Information Available: Table S1, giving crystal data collection and processing parameters, Figure S1, giving the proton NMR spectrum of compound **6**, and crystallographic data as CIF files for complexes **6, 7**, **9**, **11**, and **13**. This material is available free of charge via the Internet at http://pubs.acs.org.

OM034189+